

# Interfacially Driven Deformation Twinning in Bulk Ag-Cu Composites

N. A. MARA,<sup>1,2</sup> I. J. BEYERLEIN,<sup>1</sup> J. S. CARPENTER,<sup>1</sup> and J. WANG<sup>1,3</sup>

1.—Los Alamos National Laboratory, Los Alamos, NM 87545, USA. 2.—e-mail: namara@lanl.gov.  
3.—e-mail: wangj6@lanl.gov

Interfaces and interface/defect interactions increasingly dominate the mechanical response of materials as the dimensions of the grains decrease to the nanoscale. Recently, we reported unusually profuse deformation twinning in Ag-Cu layered eutectic composites with bilayer thicknesses in the submicron regime (~200 nm–400 nm) at room temperature and low strain rates. Using atomistic simulations and dislocation theory, we propose that the Ag-Cu interface facilitated deformation twinning in Cu by permitting the transmission of twinning partials from Ag to Cu. In this way, twins in Ag can provide an ample supply of twinning partials to Cu to support and sustain twin growth in Cu during deformation. Interface-driven twinning as revealed by this study suggests the exciting possibility of altering the roles of dislocation slip and twinning through the design of heterophase interface structure and properties.

## LAMELLAR COMPOSITES AT THE NANOSCALE

The concept of using lamellar composites to enhance material behavior has been one that has endured the test of time. For example, plywood made by the ancient Egyptians over 5,000 years ago, and pattern welded steel, from about 300 BC, are still in use today as either major components of our construction industry or as decorative knife blades, but these products have become more sophisticated with the use of more exotic starting polymers or metal alloys. Regardless of these advances, the critical intrinsic length scale, in this case, layer thickness, is always on the order of microns or greater, and so the improvement in mechanical properties is typically due to the interactions between the multiple phases.

To date, investigations into metallic lamellar composites where the individual layer thicknesses are 100 nm or less (nanolamellar composites) revealed that as layer thicknesses decrease, remarkable improvements arise in damage resistance under mechanical loading or ion irradiation.<sup>1–10</sup> For instance, with decreasing layer thickness, strength can rise from just a few tens of MPa in the case of nominally soft high symmetry metals such as Cu, Nb, Ni, or Ag, to a few GPa when they are combined into a lamellar composite, and it can approach the

theoretical strength of the material, which is defined as the strength of the material without the mechanical advantage afforded by dislocation motion, approximately the shear modulus/30. The reasons that nanoscale-layer thicknesses lead to unprecedented results have yet to be clarified. In this pursuit, our interests lie in the role interface properties play in governing material deformation behavior.

Regarding plastic deformation, two basic deformation mechanisms, dislocation slip and deformation twinning, provide most of the permanent deformation in face-centered cubic (fcc) crystalline solids. The strong dependence of twinnability on stacking fault energy leads materials such as Ag, which have a low stacking fault energy ( $19 \pm 3$  mJ/m<sup>2</sup>),<sup>11,12</sup> to twin readily, whereas medium stacking fault energy materials such as Cu (36 mJ/m<sup>2</sup> and higher)<sup>13–15</sup> tend not to twin as easily, especially under low strain rate, room-temperature conditions. Cu has been experimentally observed to undergo deformation twinning under specialized high-stress conditions such as high strain rates, low temperatures, or at very small grain sizes less than 20 nm.<sup>16–23</sup> Similarly, deformation twinning is evident in molecular dynamics simulations of Cu,<sup>24,25</sup> where grain sizes are  $\leq 10$  nm. Zhu et al.<sup>26</sup> predicted that the optimum grain size for deformation twinning for Cu undergoing a grain boundary partial

dislocation emission mechanism is 38 nm to 54 nm. Without satisfying the above conditions, deformation twinning in copper does not occur if either grain sizes or layer thicknesses are of 100 nm or greater.

The majority of the above work was carried out on single-phase systems. However, we have seen differences for propensity of deformation twinning of Cu in the Cu-Nb nanolamellar system by simply changing the interface structure and crystallography, keeping length scales and deformation conditions constant.<sup>27</sup> This leads to the hypothesis that not only microstructural length scales and deformation conditions but also the structure of the interface and the deformation mechanisms those structures enable have an impact on twinnability. In the Cu-Nb work, twin nucleation depends on the ability of the interface to readily supply twinning partial dislocations via dissociation reactions and interactions with incoming full dislocations.<sup>28</sup> This leads to a natural extension of this hypothesis to investigation of a material system where one phase, Ag, undergoes deformation largely through deformation twinning, and the other, Cu, is much more reluctant to twin. If, at the interface, transmission or twin communication events take place that can facilitate twinning in the harder-to-twin phase, the phenomena of interface dominance can be further investigated. In this work, we investigated Ag-Cu bulk cast eutectic in nanolamellar form, and the effects of the Ag-Cu interface on deformation twinning in Cu.

### BULK CAST NANOLAMELLAR AG-CU EUTECTIC

#### Synthesis and Characterization of Microstructure

A particular challenge in working with nanocomposites is the lack of well-controlled synthesis routes for producing bulk amounts ( $\text{cm}^3\text{s}$ ) of material. Much

of the work in the literature (for a review, see Ref. 9) focuses on vapor-deposited foils, which are ideal for the ion irradiation experiments, thermal stability measurements, and nanomechanical testing that has revealed the unique structure/property relationships found in this class of materials. However, techniques such as accumulative roll bonding (ARB),<sup>4,5,29</sup> repeated wire drawing and bundling,<sup>30,31</sup> and casting of eutectics<sup>32,33</sup> have been found to be effective in synthesizing bulk amounts of wire, sheet, or rod. Ag-Cu eutectic is an ideal model system for investigating fcc/fcc nanocomposites, and it consists of a 60/40 at.% Ag/Cu composition, immiscibility between the phases at room temperature, and the ability to generate a microstructure containing interfaces with either a cube-on-cube orientation relationship or twin orientation relationship and  $\{111\}\text{Ag}/\{111\}\text{Cu}$  interface planes.<sup>34</sup> Through the use of deep undercooling of ultrahigh-purity starting materials via melting and subsequent water quenching described elsewhere<sup>32</sup> material with average 200-nm lamellar thickness can be cast into rods of 9 mm diameter. The resulting typical eutectic microstructure consists of randomly oriented colonies containing alternating lamellae of Cu and Ag, as seen in Fig. 1, where Fig. 1a is a scanning electron microscope (SEM) micrograph of a single central Ag-Cu colony with nearly parallel lamellae, and Fig. 1b is a cross-sectional transmission electron microscopy (TEM) micrograph of one such colony showing the alternating Cu and Ag layers. The selected area diffraction pattern shown in Fig. 1c reveals the cube-on-cube orientation relationship, as well as the dominant  $\{111\}\text{Cu}/\{111\}\text{Nb}$  interface plane normal. Consistent with other findings in the literature,<sup>34</sup> Ag shows diffraction spots corresponding to growth twins parallel to the  $\{111\}$  interface plane designated as  $\text{Ag}_2$ .

The high-resolution TEM (HRTEM) micrograph of Fig. 2a further elucidates the local structure of the interface, which not only consists of matching

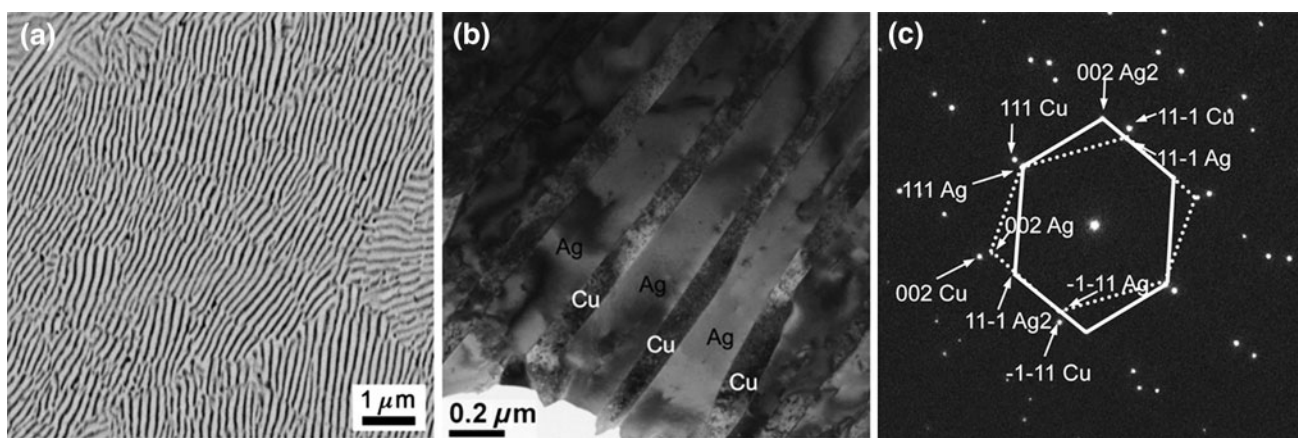


Fig. 1. Electron micrographs of the as-cast eutectic microstructure. (a) SEM micrograph showing a central Ag-Cu lamellar colony and surrounding colonies at differing crystallographic orientation. (b) Cross-sectional TEM micrograph of such a colony showing alternating Ag and Cu layers. (c) SADP of the area in (b) showing the cube-on-cube orientation relationship and  $\{111\}$  Ag-Cu interface plane, as well as twinning in Ag parallel to the interface plane.

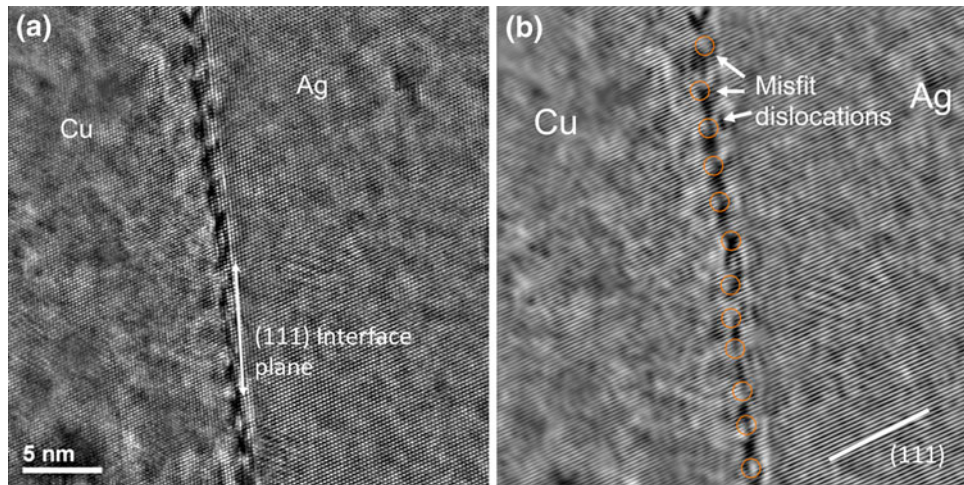


Fig. 2. (a) HRTEM micrograph of Ag-Cu (111) interface in the as-cast condition. (b) Inverse fast Fourier transform image highlighting the (111) planes and misfit dislocations associated with relieving coherency strains due to lattice parameter mismatch.

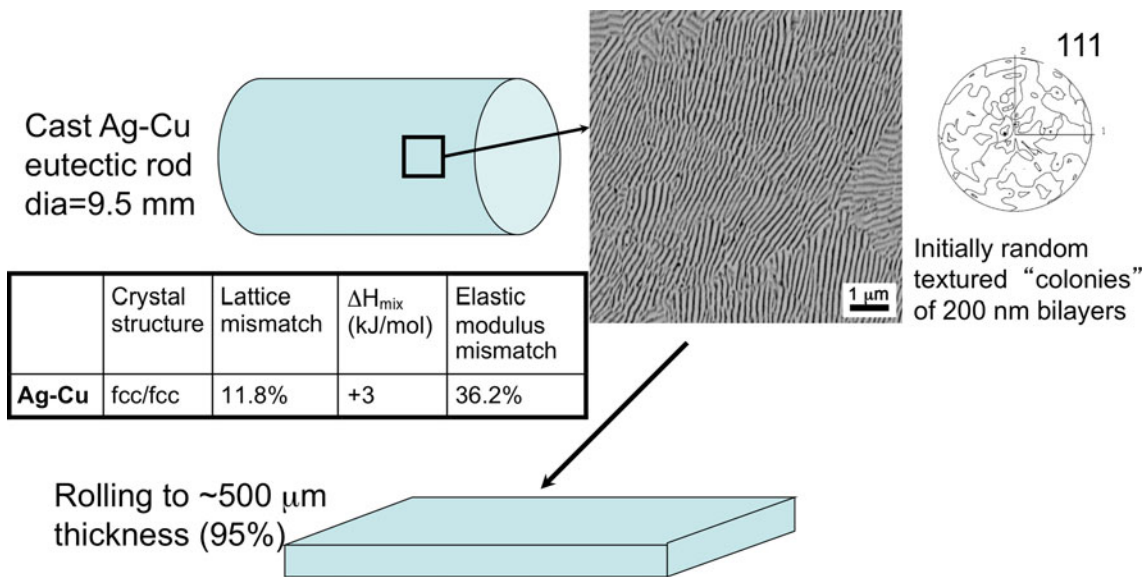


Fig. 3. Processing of Ag-Cu nanocomposite, starting with 9.5-mm diameter cast eutectic rod consisting of randomly oriented colonies of 200-nm bilayers, then rolled to 500- $\mu\text{m}$  thickness. Inset table shows crystal structure, lattice mismatch, heat of mixing, and elastic modulus mismatch for Ag-Cu.

{111} planes of Cu and Ag, but also has a series of misfit dislocations and disconnections, highlighted through inverse fast Fourier transform image processing as in Fig. 2b. This series of intrinsic interfacial defects vary nonuniformly from 9 to 11 lattice planes in Cu (1.991 nm to 2.433 nm) and from 8 to 10 lattice planes in Ag (1.998–2.497 nm) along the interface. The disconnections, or steps, in the interface, are spaced roughly every five misfit dislocations (99.25–110.3 nm). These misfit dislocations arise from accommodating the lattice spacing mismatch of 11.8% between Cu and Ag.

### Mechanical Response During Rolling

After casting, the 9.5-mm diameter Ag-Cu cast eutectic rods were rolled to a minimum reduction in

thickness of 75% based on the initial rod diameter. Rolling was carried out at both room temperature and 200°C, with no detectable difference in processing behavior. Figure 3 shows a schematic of this process, as well as a table listing some basic properties of the Ag-Cu system and geometry of the sample. As shown in the inset pole figure, the initial colony texture distribution is random. After rolling, however, this texture changes substantially. During deformation processes, certain slip systems will be favored under a given loading scenario due to higher resolved shear stresses being applied to favored slip systems, and the dominant deformation mechanism(s) at hand. This in turn determines the degree and direction of crystal rotation that the individual grains or in this case, colonies, will undergo during deformation. The distribution of



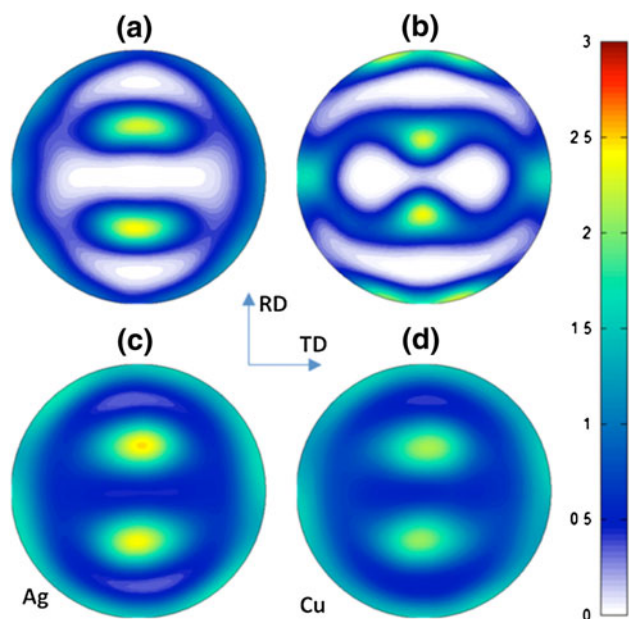


Fig. 4. Calculated (111) pole figures of textures for a model fcc metal with (a) slip and at least 30% of the phase reoriented via twinning and (b) slip only. X-ray diffraction measured (111) pole figures of the textures of Ag and Cu within the Ag-Cu composite after rolling to 75% reduction at room-temperature (c) Ag and (d) Cu. The transverse direction (TD) is the horizontal direction, the rolling direction (RD) is the vertical direction, and contour levels are 1.0/1.4/2.0/2.8 mrd.

crystal orientations after deformation processing defines its crystal texture, and for a given deformation pathway and crystal structure, characteristic textures can arise. In the case of fcc metals undergoing room-temperature rolling deformation to large strains, two commonly encountered textures are presented in Fig. 4a, b. Figure 4a presents the expected {111} pole figure that is commonly associated with materials such as Ag, where dislocation slip is accompanied by a significant fraction of deformation twinning, at least 30% twin fraction. Figure 4b is that for a material that does not undergo deformation twinning and is typically seen for materials such as Al or Cu that do not twin but deform via dislocation slip only. After comparing these with the measured {111} pole figures in Fig. 4c, d for Ag and Cu, respectively, it is clear that (I) both Ag and Cu deformed by similar mechanisms, as indicated by their similar textures, and (II) both Ag and Cu have developed textures expected from a material undergoing heavy amounts of deformation twinning (e.g., over 30% twin volume fraction).

The codeformation of Ag and Cu is further supported by in situ neutron diffraction during compression testing, carried out at the Los Alamos Neutron Science Center (LANSCE). Figure 5 shows a plot of microstrain measured by change of d-spacing for the various crystal planes in Cu and Ag versus the macrostrain measured via crosshead displacement. The planes are (220), (111), (311), and

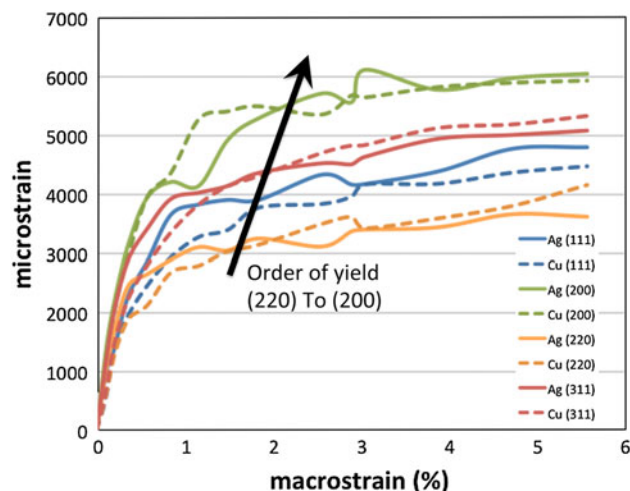


Fig. 5. Plot of microstrain versus macrostrain for Ag-Cu nanolamellar eutectic during in situ compression testing in the neutron beam. Note that each set of planes in Cu (dashed) yields simultaneously with the same set of planes in Ag (solid).

(200). The in situ neutron diffraction data measure elastic strain between these planes as deformation progresses. The onset of plastic slip on a given set of slip planes is indicated by a transition from linear elastic behavior to “saturation,” since no additional microstrain is measured as a function of increasing applied macrostrain. The smooth transition indicates that slip initiates in a distributed fashion over a finite amount of strain. From this plot, we can ascertain the order of yielding in certain crystallographic directions is (220), (111), (311), and (200) for both Ag and Cu. In other words, the onset of plasticity on a given set of planes in Cu closely follows that in Ag. This means that the degree of elastic strain, as well as the onset of yield in Ag, is mirrored by that in Cu.

Based on these findings, we can postulate that in this ultrafine lamellar composite, Ag and Cu codeform via the same mechanisms, be it slip or twinning and even more remarkably, the Cu phase can deformation twin just as intensely as Ag, in spite of the fact that rolling takes place at room temperature and low strain rates. Such unusual behavior in Cu is likely a result of being joined to Ag and the Ag-Cu interface. In light of these results, we further hypothesize that twinning partials in Cu are either transmitted across or directly nucleated from the Ag-Cu interface, leading to the observed twinning in the Cu phase.

The x-ray texture measurements and corresponding pole figures are indicative of a bulk response, and so a careful TEM study was carried out to determine the local effects of rolling deformation, with a special emphasis on quantifying the amount of twinning occurring in Cu, as well as the effects of the interface on twinning mechanisms. Figure 6a, c are bright-field TEM micrographs of one of the colonies after rolling to 75% reduction. The accompanying SADP in

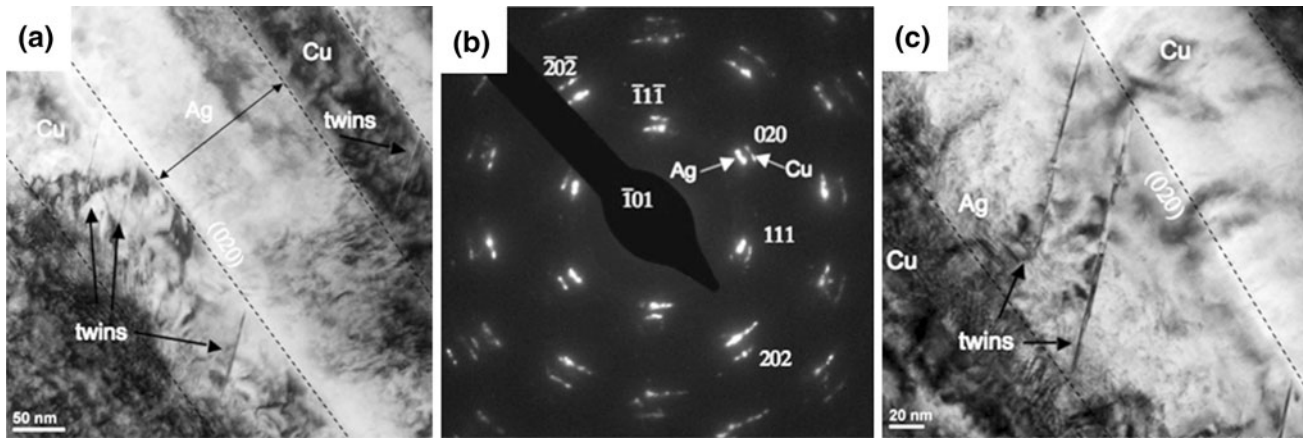


Fig. 6. TEM analysis of Ag-Cu layered eutectic composites after rolling to 75% reduction: (a) and (c) TEM bright-field image of Ag and Cu lamellae. (b) Diffraction pattern from the same region showing a  $\langle 101 \rangle$  zone axis pattern. The interface plane trace has a normal along (020) and is parallel to [202]. Fine twins are indicated in the Cu layer (a) and in the Ag layer (c).

Fig. 6b indicates that the cube-on-cube orientation relationship across the interface has been retained, which is consistent with the x-ray diffraction texture findings. However, the interface plane normal has rotated from a  $\{111\}$  initial interface plane to a  $\{010\}$  interface plane after rolling. Such a rotation of the interface plane, from a geometric standpoint, is consistent with complete twinning of both the Cu and Ag phases.<sup>35</sup> In other words, both the Cu and Ag crystals on either side of the interface have twinned fully. This is consistent with their deformation textures, characteristic of heavily twinned Cu and Ag. Also evident are very fine twins emanating from the  $\{010\}$  interface and occurring equally in the Ag and Cu (Fig. 6c). These are at most a few atomic layers thick and do not appear in enough quantity to be detected via a bulk texture measurement. Thus, primary twinning caused the reorientation of the interface to  $\{010\}$  and the new  $\{010\}$  interface are forming secondary twins in the Cu and Ag phases.

### TWINNING MECHANISMS

The above argument for reorientation of the interface plane from  $\{111\}$  to  $\{010\}$  relies on an abundance of twinning partials of similar variants to drive twinning in both Ag and Cu phases. Should the neighboring Ag and Cu crystals both twin by the same twin variant, it can be shown via a matrix transformation<sup>35</sup> that the shared  $(111)_M$  interface plane (where the subscript M corresponds to coordinates in the original crystal) will reorient to either the  $(001)_T$  or  $(111)_T$  plane (where the subscript T corresponds to coordinates in the twinned crystal). Consider the  $(111)_M$  plane as the original Ag-Cu interface plane and the  $(11\bar{1})_M$  plane as twinning plane in Ag. The three possible twinning partials (variants) that can construct an fcc twin on plane  $(11\bar{1})_M$  are denoted as  $\mathbf{b}_1$ ,  $\mathbf{b}_2$ , and  $\mathbf{b}_3$ . Due to their screw/edge character,  $\mathbf{b}_1$ ,  $\mathbf{b}_2$ , and  $\mathbf{b}_3$  belong to one of two possible sets. Set I includes  $\mathbf{b}_1$ , which is pure

edge,  $\mathbf{b}_1 = \frac{a}{6}[112]$ . Through the glide of set I the interface plane will reorient to  $(001)_T$ . Set II includes both  $\mathbf{b}_2$  and  $\mathbf{b}_3$ , which have the same edge component but opposite-sign screw components, i.e.,  $\mathbf{b}_2 = \frac{a}{6}[\bar{2}1\bar{1}]$  or  $\mathbf{b}_3 = \frac{a}{6}[1\bar{2}\bar{1}]$ . Through the glide of set II, the interface plane will reorient to  $(111)_T$ . It is worth mentioning that an alternating stack of  $\mathbf{b}_2$ : $\mathbf{b}_3$  partials is expected to be more energetically favorable than a stack of  $\mathbf{b}_2$  partials or  $\mathbf{b}_3$  partials alone since the composite  $\mathbf{b}_2$ : $\mathbf{b}_3$  structure cancels the long-range screw dislocation fields. The important implication of the reorientation analysis is that the layers bounded by the  $\{010\}$  Ag-Cu interface planes in the TEM micrographs in Fig. 6, twinned entirely. If this were the case, then the volume fraction of material twinned would be detected via a bulk texture measurement, which is consistent with experimental observation. Based on the above analysis, it is highly likely that the  $\{010\}$  interface plane and cube-on-cube orientation relationship results from twinning in both Cu and Ag by the same twinning system. This implies that the fine twins connected to the  $\{010\}$  Ag-Cu interface in Fig. 6 are in fact secondary twins, not primary twins. With that said, the key issues to be addressed next are the mechanisms for the nucleation and growth of Cu twins that match neighboring Ag twins and the kinetics and energetics involved in these processes.

For a molecular dynamics (MD) simulation to address the mechanisms behind this behavior, two observations must be addressed: Primary twinning, which is responsible for the prolific twinning in both Cu and Ag, results in bulk reorientation of the interface (Fig. 6a). Secondary twinning is exhibited by the fine twins in the reoriented Cu matrix (Fig. 6c). Here, we address two possible mechanisms that can occur at an atomic scale: twin transmission across the interface and twin nucleation from an existing defect source at the interface. The first mechanism allows for the Ag phase to provide an ample source of twinning partials that transmit



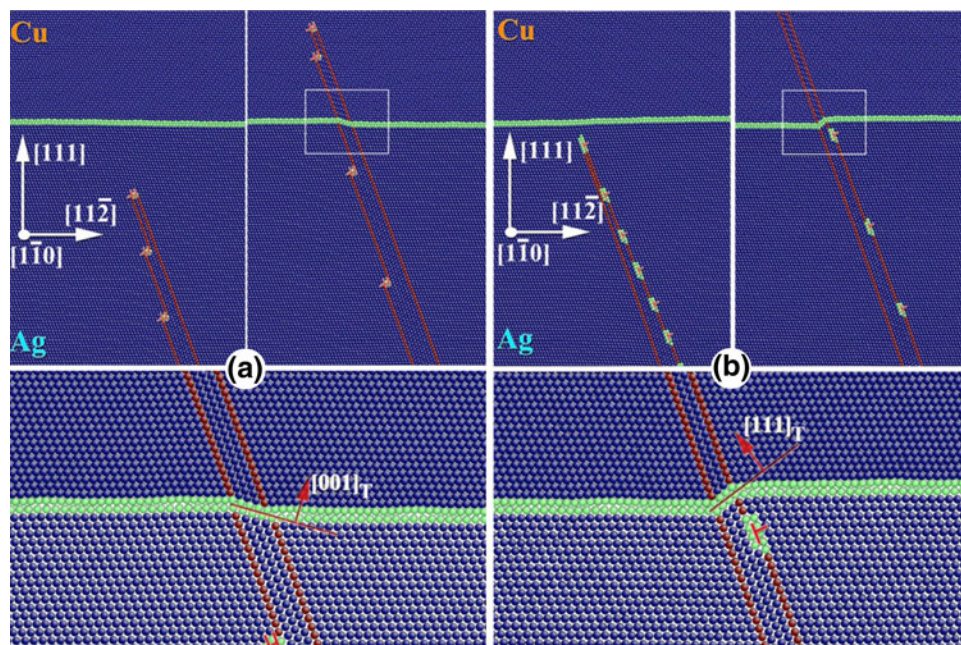


Fig. 7. Atomistic simulations of twin transmission across the Ag-Cu interface at a resolved shear stress of 100 MPa at room temperature: (a) An 8-layer twin (created through the glide of a set of partials  $b_2$  and  $b_3$ ) in Ag crosses a (111) Ag-Cu interface: the initial configuration, a 4-layer twin in Cu, and the resultant interface plane (001)<sub>T</sub>; and (b) A 6-layer twin (created through the glide of a set of partials  $b_4$ ) in Ag crosses a (111) Ag-Cu interface: the initial configuration, a 3-layer twin in Cu, and the new interface plane (111)<sub>T</sub>. The subscript “T” corresponds to the coordinates in the twinned crystal. The vector  $\mathbf{n}$  is the normal direction of the resultant interface plane. Atoms are colored according to common-neighbor-analysis. Blue atoms represent fcc structure, red atoms represent hcp structure, and green atoms represent a defective structure. The symbol “ $\perp$ ” represents a dislocation (Color figure online).

across the interface into Cu, which is in agreement with the natural propensity for Ag to twin in bulk form. The second mechanism is more likely to explain the relatively small amount of secondary twinning that has been observed after the primary twinning event has taken place.

Figure 7a, b address the transmission event via MD simulation of both Set I (Fig. 7a) and Set II (Fig. 7b), respectively. The initial Ag-Cu interface is free of extrinsic defects, and it contains only the misfit dislocations required to reduce the coherency strains. Details behind the simulation can be found in Ref. 36. The transmission of set I dislocations shown in Fig. 7a agrees well with the reorientation of the interface plane to (001) as seen in the experiment. In this case, as a multilayered twin in Ag transmits across the interface, the interface plane reorients to (010) and leaves a set of small residual dislocations, as well as a small rotational deviation from the (010) interface of  $1.1^\circ$ .<sup>37</sup> In comparison, the transmission of set II dislocations leaves a newly oriented (111) interface plane, residual dislocation content, and a rotational deviation from the (111) interface of  $2.2^\circ$ . Clearly, the transmission of set I dislocations agrees with the experiment, but it is a reasonable mechanism on an energetic basis due to the lower energy penalties associated with both an advancing set I twin front and with the set I post-transmission residual dislocation content. The process described above leaves a set of small residual

dislocations at the new (010) interface. Such a set of dislocations with small individual Burgers vectors will be driven to rearrange to recover coherency over large portions of its area.<sup>38</sup>

To discuss these reactions, the residual dislocations are described in terms of their in-plane and out-of-plane components:  $b_{rx}$ , lying parallel to and  $b_{ry}$ , lying perpendicular to the interface plane. For the {010}-type interface plane formed by set II twin transmission, the in-plane component  $b_{rx}$  of the residual dislocations has the same sign as the pre-existing misfit dislocations  $b_m^{\{111\}}$  (with Burgers vector  $\frac{1}{6}\langle 112 \rangle$  and average spacing of 2 nm<sup>37</sup>) associated with the original {111} interface. The components  $b_{rx}$  from multiple tiny residuals are driven to combine via interfacial glide with  $b_m^{\{111\}}$  in order to form the misfit dislocations associated with the new {010} interface, denoted  $b_m^{\{100\}}$  (with larger Burgers vector  $\frac{1}{2}\langle 110 \rangle$ , and the spacing of 2.5 nm<sup>37</sup>). Unlike the misfit  $b_m^{\{111\}}$  belonging to the original {111} plane,  $b_m^{\{100\}}$  is a Lomer dislocation that can undergo a nonplanar dissociation into two twinning partials plus a stair-rod dislocation at interface,<sup>15,37,39</sup> as illustrated at the bottom of Fig. 8a.

Another mechanism for recovery involves the out-of-plane components  $b_{ry}$  of the residual dislocation array. The  $b_{ry}$  of multiple residual dislocations can combine to form a large interfacial disconnection  $b_{Ry}$ . This disconnection  $b_{Ry}$  can act as a source and emit Shockley partial dislocations into one or both of

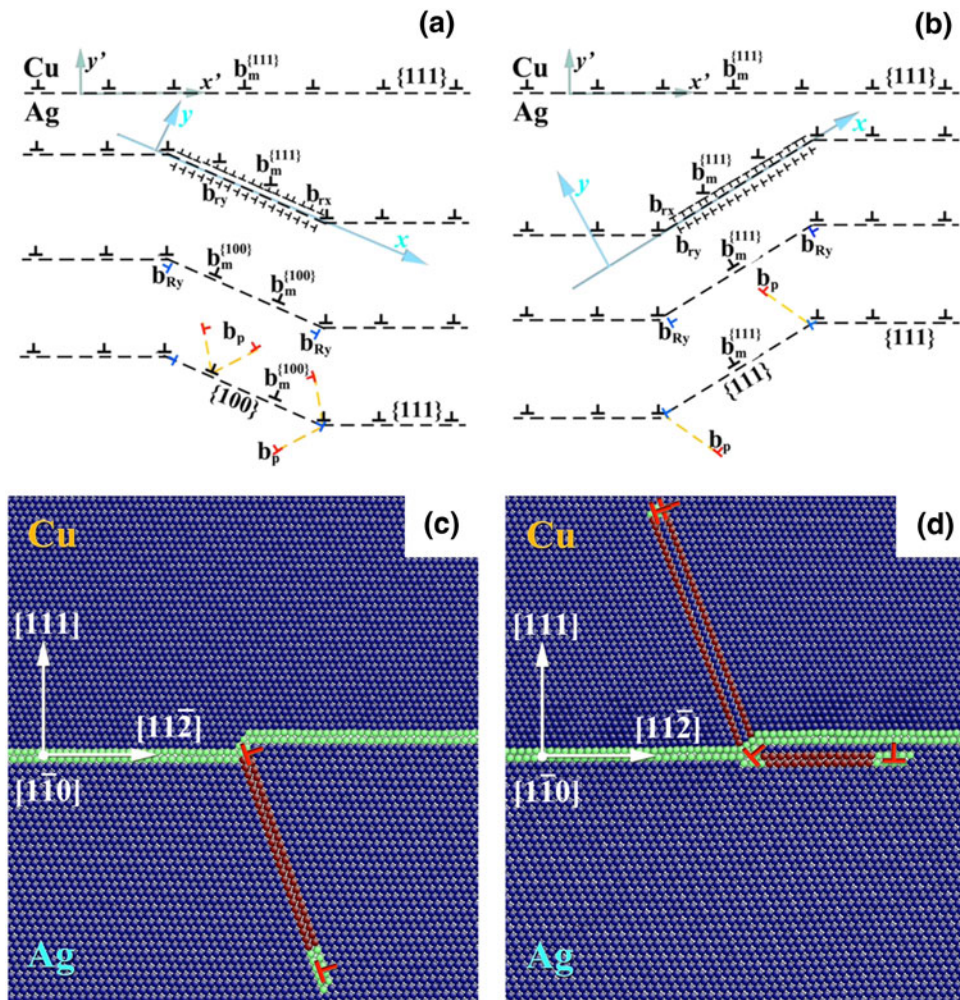


Fig. 8. Schematic of the reaction mechanisms between the residual dislocations remaining after the transmission events and the misfit dislocations pre-existing at the interface (a) for the new  $\{100\}$  interface plane and (b) new  $\{111\}$  interface plane. (c and d) Atomistic simulations showing the formation of a 2-layer thick twin in Cu as a result of the interaction of a lattice dislocation with an interface disconnection: (c) initial configuration and (d) final configuration. Atoms are colored according to common-neighbor analysis. Blue atoms represent fcc structure, red atoms represent hcp structure, and green atoms represent a defective structure. The symbol “ $\perp$ ” represents a dislocation (Color figure online).

the adjoining Ag and Cu crystals. For demonstration, Fig. 8c, d show the formation of a two-layer thick twin in Cu as a result of the reaction of a lattice dislocation with a  $\{111\}$  interface disconnection.

The two recovery mechanisms described above explain the fine twins that appeared in the Ag and Cu layers in connection with the  $\{001\}$  interfaces in the deformed material. The reduction in the magnitude of the out-of-plane component of the residual interfacial dislocations via emission of twinning partials reduces the tilt, restoring the cube-on-cube orientation relationship and the excess energy at the interface.

For completeness, we show in Fig. 8b the recovery mechanism for the reoriented  $\{111\}$ -type interface plane as a result of set II twin transmission. Although, in this case, the misfit dislocations associated with the newly created interface have the same type Burgers vector as the preexisting misfit

dislocations (both are  $1/6\langle 112 \rangle$ ), the combination of  $b_{rx}$  and the preexisting misfit dislocations is energetically favored because they are opposite in sign. As with the  $\{010\}$ -type interface plane, Shockley partial dislocations can emit into one or both of the adjoining Ag and Cu crystals from interfacial disconnections  $b_{ry}$ , formed when the tiny residual dislocations  $b_{ry}$  combine.

The present MD simulations reveal two ways in which the interface can promote deformation twinning in Cu, with the added significance that such assistance does not require extreme stresses associated with shock loading, cold temperatures, 1 nm–10 nm length scales, or severe stress concentrators, like cracks. The two mechanisms for Cu twinning observed in simulation, (I) twin partials transmission from Ag to Cu and (II) twin partial nucleation from an interfacial step, are elementary in nature. When repeated in succession, either unit process can potentially grow the twin within the layer.



These mechanisms introduce leading twinning partials only into the Cu phase. Trailing partials that would otherwise correct the twin fault and shut down twin formation are not present. Notably, the proposed transmission mechanism can ease both twin nucleation and growth in Cu, and it can explain the observed Ag-Cu interface transformation to the {100} plane and the fine twins in both Ag and Cu after deformation.

### DISCUSSION OF THE STRUCTURE-ENERGY-KINETICS TRIAD

In the Ag-Cu system, twinning partial transmission and subsequent recombination of residual dislocations were found to be the dominant deformation mechanism during room temperature rolling where lamellar thicknesses are between 100 nm and 200 nm, a regime where deformation twinning is unexpected. This differs from the mechanisms exhibited by the Cu-Nb system explained in the leading article of this series, which relies on dissociation of intrinsic dislocations at the interface to aid in twin nucleation. As such, interfaces that differ in their structure, energetics, and kinetics give differing mechanical responses. This, in turn, offers the opportunity to engineer materials with tailored properties under extreme environments (mechanical and radiation).

Under the subheadings of structure, energetics, and kinetics (see the triad explained in the earlier article by Beyerlein et al.<sup>40</sup>), the Ag-Cu system has its own set of interfaces with its own mechanisms that drive deformation twinning in Cu. The structure of the Ag-Cu interface is derived from a cube-on-cube orientation relationship with a {111}Ag//{111}Cu interface plane. As seen in Fig. 2, the 11.8% mismatch in lattice spacing is accommodated by a regular array of dislocations and disconnections. This structure, in and of itself, should not aid but does not necessarily hinder twinning in Cu. The interface also should not contribute favorably to the energetics of twinning in Cu in any way because the Burgers vector of the misfit dislocation array in Cu does not have an out-of-plane component that can contribute via dissociation to forming a twinning partial. However, this energetics argument changes as the interface reorients into a {010} type interface, where now the recombination of residual dislocations leads to a misfit dislocation structure that can contribute to twinning partial emission via dissociation events. That is, the {010} Ag-Cu interface can contribute energetically to twin formation, whereas the {111} interface does not. In the case of the {111} Ag-Cu interface, however, the kinetics of transmissibility should prove to be favorable. The mechanisms presented in the MD simulations rely on the transmissibility of twinning partials, which is enabled by the cube-on-cube orientation relationship that leads to close alignment of all slip systems in both phases. A similar argument applies to the

{010} Ag-Cu interface, where the alignment of slip systems only adds to the ability of this interface to facilitate twinning in Cu.

### ACKNOWLEDGEMENTS

This work was supported as part of the Center for Materials at Irradiation and Mechanical Extremes, an Energy Frontier Research Center funded by the U.S. Department of Energy, Office of Science, Office of Basic Energy Sciences under Award Number 2008LANL1026. A portion of this research was performed on the SMARTS instrument at the Lujan Center at Los Alamos National Laboratory supported by DOE-BES under FWP #2012LANLE389. The authors gratefully acknowledge useful discussion and collaboration with Dr. Dhriti Bhattacharyya.

### REFERENCES

1. M.J. Demkowicz, P. Bellon, and B.D. Wirth, *MRS Bull.* 35, 992 (2010).
2. M.J. Demkowicz, R.G. Hoagland, and J.P. Hirth, *Phys. Rev. Lett.* 100, 136102 (2008).
3. D. Bhattacharyya, N.A. Mara, P. Dickerson, R.G. Hoagland, and A. Misra, *Acta Mater.* 59, 3804 (2011).
4. J.S. Carpenter, X. Liu, A. Darbal, N.T. Nuhfer, R.J. McCabe, S.C. Vogel, J.E. Ledonne, A.D. Rollett, K. Barmak, I.J. Beyerlein, and N.A. Mara, *Scr. Mater.* 67, 336 (2012).
5. J.S. Carpenter, S.C. Vogel, J.E. Ledonne, D.L. Hammon, I.J. Beyerlein, and N.A. Mara, *Acta Mater.* 60, 1576 (2012).
6. N.A. Mara, D. Bhattacharyya, J.P. Hirth, P. Dickerson, and A. Misra, *Appl. Phys. Lett.* 97, 021909 (2010).
7. N.A. Mara, A. Misra, R.G. Hoagland, A.V. Sergueeva, T. Tamayo, P. Dickerson, and A.K. Mukherjee, *Mater. Sci. Eng. A* 493, 274 (2008).
8. A. Misra, M.J. Demkowicz, X. Zhang, and R.G. Hoagland, *JOM* 59, 62 (2007).
9. A. Misra, and R.G. Hoagland, *Encyclopedia of Nanoscience and Nanotechnology*, ed. H.S. Nalwa (Valencia, CA: American Scientific Publishers, 2005).
10. N.A. Mara, D. Bhattacharyya, P. Dickerson, R.G. Hoagland, and A. Misra, *Appl. Phys. Lett.* 92, 231901 (2008).
11. H. Suzuki and C.S. Barrett, *Acta Metall.* 6, 156 (1958).
12. E.B. Tadmor and N. Bernstein, *J. Mech. Phys. Solids* 52, 2507 (2004).
13. C.B. Carter and I.L.F. Ray, *Philos. Mag.* 35, 189 (1977).
14. P. Coulomb, *Scr. Metall.* 15, 769 (1981).
15. J.P. Hirth and J. Lothe, *Theory of Dislocations* (New York: Krieger Publishing Company, 1982).
16. C.X. Huang, K. Wang, S.D. Wu, Z.F. Zhang, G.Y. Li, and S.X. Li, *Acta Mater.* 54, 655 (2006).
17. M.A. Meyers, O. Vohringer, and V.A. Lubarda, *Acta Mater.* 49, 4025 (2001).
18. J.C. Sanchez, L.E. Murr, and K.P. Staudhammer, *Acta Mater.* 45, 3223 (1997).
19. W. Yinmin, J. Tong, and M. En, *Mater. Trans.* 44, 1926 (2003).
20. X.Z. Liao, Y.H. Zhao, S.G. Srinivasan, Y.T. Zhu, R.Z. Valiev, and D.V. Gunderov, *Appl. Phys. Lett.* 84, 592 (2004).
21. X.Z. Liao, Y.H. Zhao, Y.T. Zhu, R.Z. Valiev, and D.V. Gunderov, *J. Appl. Phys.* 96, 636 (2004).
22. X.Z. Liao, F. Zhou, E.J. Lavernia, D.W. He, and Y.T. Zhu, *Appl. Phys. Lett.* 83, 5062 (2003).
23. C. Mingwei, M. En, K.J. Hemker, S. Hongwei, W. Yinmin, and C. Xuemei, *Science* 300, 1275 (2003).
24. J. Schiotz, F.D. Di Tolla, and K.W. Jacobsen, *Nature* 391, 561 (1998).
25. H. Van Swygenhoven, P.M. Derlet, and A. Hasnaoui, *Phys. Rev. B* 66, 024101/1 (2002).
26. Y.T. Zhu, X.Z. Liao, S.G. Srinivasan, and E.J. Lavernia, *J. Appl. Phys.* 98, 34319 (2005).



27. I.J. Beyerlein, N.A. Mara, D. Bhattacharyya, D.J. Alexander, and C.T. Necker, *Int. J. Plast.* 27, 121 (2011).
28. W.Z. Han, J.S. Carpenter, J. Wang, I.J. Beyerlein, and N.A. Mara, *Appl. Phys. Lett.* 100, 011911 (2012).
29. P.H. Shingu, K. Yasuna, K.N. Ishihara, A. Otsuki, and M. Terauchi, *Kiritani Symposium on Structural Defects in Advanced Materials* (Switzerland: Gordon & Breach, 1996).
30. L. Thilly, F. Lecouturier, and J. Von Stebut, *Acta Mater.* 50, 5049 (2002).
31. L. Thilly, P.O. Renault, V. Vidal, F. Lecouturier, S. Van Petegem, U. Stuhr, and H. Van Swygenhoven, *Appl. Phys. Lett.* 88, 191906 (2006).
32. T.D. Shen, R.B. Schwarz, and X. Zhang, *Appl. Phys. Lett.* 87, 1 (2005).
33. T.D. Shen, X. Zhang, K. Han, C.A. Davy, D. Aujla, P.N. Kalu, and R.B. Schwarz, *J. Mater. Sci.* 42, 1638 (2007).
34. J.B. Liu, Y.W. Zeng, and L. Meng, *J. Alloys Compd.* 464, 168 (2008).
35. M. Niewczas, *Dislocations in Solids*, ed. F.R.N. Nabarro and J.P. Hirth (New York: Elsevier, 2007), Chapter 75, p. 263.
36. J. Wang, I.J. Beyerlein, N.A. Mara, and D. Bhattacharyya, *Scr. Mater.* 64, 1083 (2011).
37. J. Wang, J.P. Hirth, R.C. Pond, and J.M. Howe, *Acta Mater.* 59, 241 (2011).
38. J.P. Hirth and R.C. Pond, *Acta Mater.* 44, 4749 (1996).
39. J.W. Christian and S. Mahajan, *Prog. Mater. Sci.* 39, 1 (1995).
40. I.J. Beyerlein, N.A. Mara, J. Wang, J.S. Carpenter, S.J. Zheng, W.Z. Han, R.F. Zhang, K. Kang, T. Nizolek, and T.M. Pollock, *JOM* (2012). doi:[10.1007/s11837-012-0431-0](https://doi.org/10.1007/s11837-012-0431-0).